Supported ruthenium nanoparticles on ordered mesoporous carbons using a cyclodextrin-assisted hard-template approach and their applications as hydrogenation catalysts

Sébastien Rio, Grégory Peru, Bastien Leger, Fatmé Kerdi, Michèle Besson, Catherine Pinel, Eric Monflier, Anne Ponchel

Supported ruthenium nanoparticles on ordered mesoporous carbons using a cyclodextrin-assisted hard-template approach and their applications as hydrogenation catalysts

Sébastien Rio[a], Grégory Peru[a], Bastien Léger[a], Fatmé Kerdi[b], Michèle Besson[b], Catherine Pinel[b], Eric Monflier[a] and Anne Ponchel[*a]

[a] Univ. Artois, CNRS, Centrale Lille, ENSCL, Univ. Lille, UMR 8181, Unité de Catalyse et de Chimie du Solide (UCCS), F-62300 Lens, France.

[b] IRCELYON, Institut de recherches sur la catalyse et l'environnement de Lyon, UMR5256 CNRS-Université Lyon 1, 2 Avenue Albert Einstein, F-69626Villeurbanne, Cedex, France

* Corresponding author: anne.ponchel@univ-artois.fr

Abstract

The present study is concerned with the preparation of ordered mesoporous carbons containing uniform dispersions of ruthenium nanoparticles by a hard-template method, based on the use of $RuCl_3$ and cyclodextrin as respective sources of metal and carbon. The influence of chemical structure of the parent CD [randomly methylated-β-CD (RAME-β-CD) and 2-hydroxypropyl-β-CD (HP-β-CD)] and loading of the ruthenium source are studied in detail. The catalysts are carefully characterized by N_2-adsorption, TEM, XRD, CO pulse chemisorption, TG-MS and H_2-TPR. The most outstanding effect is obtained when HP-β-CD is used, allowing to stabilize small and reactive Ru particles (1-2 nm) in the carbon matrix, with a good compromise between immobilization, surface availability and hydrogen spillover effect. The catalytic systems prepared from HP-β-CD display remarkably high catalytic activities in the liquid-phase hydrogenation of various substrates while their reusability and robustness are also demonstrated.

Keywords

• Cyclodextrins • Metal nanoparticles • Ordered mesoporous carbons • Confinement effect • Hydrogenation

1. Introduction

Carbon-supported noble metal catalysts are widely known for their use in practical catalytic processes for organic synthesis or fine chemical industry. Numerous methods of preparation including impregnation [1-4], ion exchange [5], colloidal deposition [6,7], chemical vapor deposition [8,9] or self-ball milling [10] have been reported for their preparation. However, the stabilization of well-dispersed metal nanoparticles (NPs) on carbon supports smaller than 2 nm is relatively difficult to obtain experimentally [11]. To improve the quality of carbon metal catalysts, efforts have been made to deposit metal NPs firmly anchored to ordered mesoporous carbon frameworks. Ordered mesoporous carbons (OMCs) are known to have a combination of ideal characteristics to be used as porous supports, with narrow pore-size distributions, large surface areas and large pore volumes. In addition, these features can be also extremely important during catalysis to afford a high diffusion of reactants and products within the pore network and promote the chemical reaction with reduced mass transfer limitation [12-14]. Since the pioneering works of Ryoo (1999) [15] and Hyeon (1999) [16], OMCs with different structural organizations, such as P*6mm*, I*m3m*, and I*a3d*, have been successfully synthesized using various mesoporous silicas as hard templates [17]. Extension of these approaches to design metal NPs well-dispersed on OMCs has been reported by different groups. For instance, Holmes et *al*. reported that cobalt NPs with a diameter of about 2-3 nm could be encapsulated in a CMK-1-type mesoporous carbon through the use of a Co-impregnated MCM-48 as template. The method involves successive steps that are: *i)* impregnation of cobalt nitrate by incipient wetness, *ii)* calcination in air followed by reduction under H_2, *iii)* filling of the pores of Co@MCM-48 by sucrose, *iv)* carbonization and finally *v)* silica dissolution in NaOH [18]. Using an organically functionalized SBA-15 silica and a hard template method, Kerdi et *al*. showed the possibility of incorporating size-controlled gold NPs in the range of 6-7 nm in CMK-3 type mesoporous carbons. Their method consisted of the immobilization of $HAuCl_4$

onto the surface of a silica chemically modified by functional coordinating groups (i.e., quaternary ammonium and mercapto groups) and *in situ* reduction with sodium borohydride to form reduced gold particles, before introducing the carbon source (sucrose) [19]. The possibility of employing a polymerizable nitrogen-rich carbon precursor for a direct incorporation of Pd NPs active for the selective oxidation of alcohols was reported by Schüth and coworkers. The synthesis of Pd-OMC composite materials with extremely small Pd clusters (<1 nm) was prepared by hard-template from the use of polyacrylonitrile to promote interaction between the palladium cations and nitrogen atoms within the silica pores during the cross linking step [20]. Beyond the effect of particle size, it has also been reported that the confinement of metal NPs within the carbon network could result in significant improvement of their catalytic performances and stronger oxidation resistance with respect to the un-encapsulated ones. For instance, Su et *al*. showed that, substantial activity enhancements (up to 24-fold compared to control Ru catalysts) were obtained in the hydrogenation of benzene and toluene by employing thermally reduced Ru NPs embedded in carbon layers or carbon supports from sucrose [21]. The thermal reduction method was defined as a method, in which the starting carbon molecule (i.e. sucrose) and its carbonized products act as *in situ* reducing agents of the metal precursor during high-temperature pyrolysis. The excellent performances were related to the dispersion of Ru NPs but also to the presence of intimate interfacial contacts between Ru and C atoms in the embedded or partially embedded NPs, facilitating the transport of hydrogen species by spillover. Similar effects were also found for catalysts prepared by different hard-template protocols [22-25]. An example of such a material was reported by Li and coworkers with the synthesis of Ru-OMC containing semi-embedded Ru NPs within the carbon structure. In this case, $RuCl_3$/SBA-15 dried at 110°C served as the hard-template while sucrose was used both as the carbon source and as the stabilizer and reductant of Ru^{3+} species. A high activity and stability for the hydrogenation of benzene could be achieved with this catalyst, being

approximately 12-fold more active than its Ru/C control [23]. The same group also reported that the addition of boric acid to the sucrose solution could help to immobilize Ru NPs with variable embedding degrees and variable impacts on the toluene hydrogenation activity [24]. Other polymerisable organic precursor than sucrose were also reported in the literature. For example, Ru NPs embedded in the OMC wall after SBA-15 replication were prepared by an auto-reduction mechanism involving the decomposition of furfuryl alcohol and $Ru(NO)(NO_3)_3$ and their activities were investigated for Fischer-Tropsch synthesis [26,27].

In line with this approach, biomass-derived sugars, such as cyclodextrins (CDs), constitute a new class of reducing organic platform molecules fully compatible with the design of nanostructured carbon-based catalysts. CDs are torus-shape molecules formed by the arrangement of α-D-glucopyranose units linked together by α-1,4 glycosidic bonds. These oligosaccharides are well-known for their ability to stabilize inclusion complexes [28-30], metallic NPs [31-33] and supramolecular adducts through the coordination of their hydroxyl groups with metal ions [34-36]. Thus, our group has established through several examples, that the association of the β-CD with a metal salt (generally nitrate) could give rise to the formation of ion-molecule adducts, which after support impregnation and calcination, have a strong impact on the final structure of the catalysts, in terms of reducibility and dispersion of active species. This was the case for Co/Al_2O_3 Fisher-Tropsch catalysts [37], Co_3O_4/ZrO_2 VOC oxidation catalysts [38,39] and Ni/Al_2O_3 alcohols amination catalysts [40]. Although CDs have also been the subject of several investigations for the synthesis of porous carbons [41-43], very little attention has been paid on their uses in the synthesis of metal-carbon composites by reverse replication. Previously, we reported that an ordered mesoporous carbon decorated by uniformly distributed Ru NPs could be obtained by carbonizing a host-guest complex formed between a randomly methylated-β-CD and adamantane carboxylic acid in the presence of $RuCl_3$ [44]. The adamantane derivative was selected as a compound capable of interacting both with

β-CD cavities and metal cations through the bicyclic structure and terminal carboxylic group, respectively. After the removal of SBA-15, the resultant Ru-C replica was shown to be highly active and stable for the hydrogenation of unsaturated fatty methyl esters.

In view of the above and as a continuation of our research towards the use of ruthenium NPs for hydrogenation reactions, herein we wish to report another example of the beneficial use of β-CDs for the preparation of ruthenium-carbon composite catalysts by the hard-template route, using $RuCl_3$ as the metal precursor. The idea is not only to use β-CD molecules as carbon sources, but also to take advantage of their natural ability to interact with metal ions by forming ion-molecule adducts [34,35] and spontaneously adsorb on mineral surfaces through hydrogen bonding (e.g. porous silica [45]). These last two factors are expected to have a positive influence on the dispersion of metal nanoparticles onto porous solid supports [37-40,46]. Also, to help control the distribution of embedded Ru nanoparticles as close as possible to the surface of the nanocomposite materials, the method is based on two successive stages of pore filling, first using a solution mixture containing the β-CD derivative and the Ru salt precursor, and second using a sucrose solution (free from metal ions). The second infiltration is rather important to ensure the complete filling of the pore system and subsequently obtain structurally ordered carbon replica after silica removal. Note that this strategy has the substantial advantage over our previous works [44] of not requiring the use of additional guest molecules, such as adamantane derivatives. Accordingly, the impact of the nature of the carbohydrate precursor and ruthenium loading on the catalytic performances is investigated and discussed on the basis of different physicochemical characterizations, including N_2 adsorption- analysis, transmission electron microscopy, X-ray diffraction, thermogravimetry, CO pulse chemisorption and temperature-programmed reduction. For water solubility purposes, the synthetic experiments focus on randomly methylated-β-CD (RAME-β-CD) and 2-hydroxypropyl-β-CD (HP-β-CD). Indeed, even if native β-CD is the most emblematic of the cyclodextrin family, it suffers from

a poor aqueous solubility (18.5 $g.L^{-1}$), preventing its use in this case. The as-obtained Ru NPs immobilized on OMCs have been employed as catalysts for the hydrogenation of various long-chain olefins and their robustness has been also evaluated.

2. Experimental section

2.1. Chemicals and reagents

Tetraethylorthosilicate (TEOS), poly(ethylene glycol)-block-poly(propylene glycol)-block-poly(ethylene glycol) [P123, ($EO_{20}PO_{70}EO_{20}$) average molecular weight, 5800], hydrochloric acid (HCl, 37 wt. %), sulfuric acid (H_2SO_4, 95 wt.%) and sucrose were purchased from Aldrich. Randomly Methylated β-cyclodextrin (RAME-β-CD; MW = 1314 $g.mol^{-1}$) with an average substitution of 12.6 methyl groups per cyclodextrin were purchased from Wacker Chemie. 2-hydroxypropyl-β-cyclodextrin (HP-β-CD; MW = 1380 $g.mol^{-1}$), which is a native β-CD partially O-2-hydroxypropylated with statistically 4.2 groups modified per cyclodextrin, was purchased from Sigma-Aldrich. The chemical structure of the cyclodextrins used in this study are gathered in Table S1 in the ESI. Ruthenium (III) chloride hydrate (40-43 wt. % Ru) was purchased from Acros Organics. Activated carbon L3S (denoted AC-L3S) supplied by CECA, France, was used as a control porous carbon support. It was produced by steam activation of pine wood and treated with nitric acid. All purchased chemicals were analytical grade and used without any further purification. Purified deionised water from Fresenius Kabi was used in all experiments.

2.2. Synthesis of SBA-15

The SBA-15 template was prepared by a microwave-hydrothermal process according to a previously published procedure [47]. 4.0 g of triblock copolymer P123 were first dispersed in 30 g of water. Then, 120 g of HCl (2 M) were added to the solution and the mixture was stirred for 2 h at 40°C to obtain a homogeneous solution. 9.0 g of TEOS were then introduced to the

previous solution which turns into a gel. The resultant gel was kept under stirring at 40 °C for 24 h before undergoing crystallization under microwave–hydrothermal conditions at 100°C for 2 h (Mars instrument, CEM Corporation, 800 watts, 2.45 GHz). The white solid was recovered by filtration, washed with water, dried overnight at 100 °C and finally calcined in a muffle furnace at 550 °C under air for 10 h. Under these synthetic conditions, SBA-15 has the following characteristics: *i)* a BJH pore diameter of 7.0 nm, *ii)* a BET specific surface area of 797 $m^2.g^{-1}$, *iii)* a pore volume of 0.83 $cm^3.g^{-1}$ and *iv)* a pore wall thickness of 4.0 nm. The pore wall thickness was calculated according the formula, $a_0 - (w_d/1.050)$, reported by Kruk et *al*., where w_d correspond to the BJH pore diameter and a_0 to the unit cell constant (10.7 nm) [48].

2.3. Synthesis of Ru-OMC nanocomposites from cyclodextrins

The Ru-containing OMC materials were prepared by a two-step replication of SBA-15. In a typical synthesis, 600 mg of β-cyclodextrin (RAME-β-CD or HP-β-CD) were added to 4.0 mL of an aqueous solution containing a precise molar amount of $RuCl_3$ and the mixture was kept for 2 h under constant stirring. Afterwards, 70 µL of H_2SO_4 (95 % wt. %) was quickly added, and then 5 min later, the mixture was allowed to infiltrate the pore of the SBA-15 template (500 mg). Subsequently, the mixture underwent polymerization at 60 °C for 24 h. The obtained silica sample, containing ruthenium and partially polymerized and carbonized cyclodextrin, was finely crushed into powder in an agate mortar before being subjected to a second pore infiltration to fill the pores completely. Note that this step was carried out with sucrose (instead of β-cyclodextrin) and without using ruthenium. More precisely, 400 mg of sucrose were dissolved in 4.0 mL of water in the presence of 45 µL of sulfuric acid and this solution was immediately used to impregnate the above-mentioned material composite. Thereafter, the material was subjected to thermo-polymerization with the following temperature program: 100°C for 6 h and 160°C for 6 h (temperatures commonly used in nanocasting processes involving sucrose) [49]. The composite was carbonized at 900 °C for 5 h under flowing

nitrogen. After washing with HF (10 wt. %) to dissolve the silica template completely, the Ru-OMC replica was successively filtered, thoroughly washed with ethanol and finally dried overnight at 100 °C.

The samples were identified according to the following notation: Ru@MC-CD(x) where CD refers to the type of cyclodextrin employed during the synthesis (RAME for RAME-β-CD and HP for HP-β-CD) and *x* corresponds to the nominal molar ratio of Ru to CD multiplied by a factor of 10. For example, Ru@MC-HP(1) indicates a Ru-OMC material prepared with an initial ratio of Ru/ HP-β-CD of 0.1 (corresponding to 4.55 mg $RuCl_3$ for 600 mg CD).

In addition, a metal-free ordered mesoporous carbon has been also prepared from randomly methylated β-cyclodextrin, using a similar manner as that previously described, except that no ruthenium salt was introduced during the synthesis. Briefly, the synthesis was carried out as follows: 600 mg of RAME-β-CD were dissolved in 4.0 mL of water and stirred for 2 h. After addition of 70 μL of H_2SO_4, the resultant solution was infiltrated into 500 mg of SBA-15. Subsequently, the mixture underwent polymerization at 60 °C for 24 h. The solid is then subjected to a second infiltration with a 4 mL aqueous solution containing 400 mg of sucrose and 45 μL of H_2SO_4 followed by polymerization at 100 and 160°C as mentioned earlier. The carbonization was carried out at 900 °C for 5 h under nitrogen flow and the subsequent silica removal was performed by HF etching. This porous carbon material was denoted as MC-RAME.

2.4. Synthesis of Ru-carbon nanocomposites from sucrose and other control materials

A ruthenium control catalyst was prepared through hard-templating in a very similar manner as the above described method, by simply replacing the cyclodextrin used during the first pore infiltration with sucrose. Without going into details, the first infiltration into the silica pores was carried out with 500 mg of SBA-15 using a mixture consisting of 4.0 mL of water, 600 mg of sucrose, 70 μL of H_2SO_4 with varying amounts of ruthenium salt, followed by a thermal

treatment at 100°C for 6 h and 160°C for 6 h. Then, the composite was treated again at 100°C and 160°C after the addition of 400 mg of sucrose and 45 µL of H_2SO_4 in 4.0 mL of water. The carbonization was completed by pyrolysis at 900°C for 5 h under nitrogen flow. The Ru-C-SiO_2 composite was washed with HF to remove the silica template and recover the template-free Ru-OMC replica, which was finally washed with ethanol, and dried overnight at 100°C. The as-obtained sample was denoted as Ru@CMK-3.

For comparison purpose, two other Ru control catalysts supported on activated carbon (Ru/AC) were prepared according to experimental procedures already detailed in the literature [50]. The synthesis of 4.2Ru/AC-L3S (Ru loading of 4.2 wt. %) consisted in the impregnation of the AC-L3S support under N_2 atmosphere at room temperature by an aqueous solution of $RuCl_3$ xH_2O. After 5 h impregnation, the catalytic suspension was treated by a formaldehyde solution and then by a KOH solution. The catalyst was filtrated, washed with distilled water until neutrality, and finally dried in an oven at 60°C under N_2. The 3.7Ru/AC-L3S-NaClO catalyst (Ru loading of 3.7 wt. %) was prepared by a cationic-exchange method carried out at room temperature under N_2 flow using AC-L3S-NaClO, which was pre-oxidized with NaOCl. The pre-treated AC-L3S-NaClO carbon support was suspended in an ammoniacal solution prior to dropwise addition of an aqueous solution $[Ru(NH_3)_6]Cl_3$. After stirring under N_2 overnight, the solid was filtered washed to neutrality, and dried under vacuum at 100°C overnight. Finally, the solid was reduced under H_2 at 300°C and passivated in 1% O_2/N_2.

2.5. Methods of characterization

Metal loadings from elemental analysis. The Ru content analysis in the solids was performed by inductively-coupled plasma optical emission spectroscopy (Horiba Jobin Yvon Activa ICP-OES).

Electrospray-mass spectrometry (ESI-MS). ESI-mass spectra were acquired from aqueous solutions containing cyclodextrin (β-CD or HP-β-CD) at 10 µM and $RuCl_3$ at 100 µM. The

experiments were conducted on a LTQ-Orbitrap XL instrument from Thermo Scientific (San Jose, CA, USA) operated in positive ionization mode with a spray voltage at +3.85 kV and an auxiliary gas flow at 45 and 15 a.u., respectively. The applied voltages were +40 V and +100 V for the ion transfer capillary and the tube lens, respectively. The ion transfer capillary was held at 275 °C and a resolution of 30,000 (m/z = 400) was applied.

Porosity measurements. Nitrogen adsorption-desorption measurements were performed at -196°C on a Micromeritics Tristar 3020 system. Prior to analysis, 100-200 mg of samples were outgassed at 300°C overnight before the measurement was performed. The data were analysed using the Tristar II 3020 V1.03 software. The specific surface areas for nitrogen adsorption were calculated using the Brunauer-Emmet-Teller (BET) model in the range of $0.01 < P/P° < 0.2$ while the pore size distributions were obtained from the adsorption branch using the Barrett-Joyner-Halenda (BJH) method. The total pore volumes were estimated at $P/P° = 0.95$ assuming that all the pores were completely filled with condensed nitrogen in the normal liquid state.

Powder X-ray diffraction (wide angle). Wide angle XRD patterns were collected at room temperature on a Bruker D8 Advance diffractometer in Bragg Brentano geometry equipped with a copper anode (λ=1.5418 Å) and a 1D PSD Lynxeye detector. The scattering intensities were measured over an angular range of $10° < 2\theta < 80°$ with a step-size of 0.02° and a counting time of 2 s per step.

Powder X-ray diffraction (low angle). Low angle XRD patterns were recorded for the ordered mesoporous materials using a Siemens D5000 equipped with a CuKα source (λ = 1.5406 Å) over an angular range of $0.3° < 2\theta < 10°$ with a step-size of 0.02° and a counting time of 1 s per step. The a_0 unit cell constants were calculated by the formula $a_0 = 2d_{100}/\sqrt{3}$.

Transmission electron microscopy. TEM performed on a Tecnai electron microscope operating at an accelerating voltage of 200 kV. The powder sample was deposited on a carbon coated copper grid before analysis. The average size of Ru nanoparticles was estimated from the size

distributions obtained from the measurement of at least 200 Ru particles using Scion Image software program.

H_2-Temperature programmed reduction (H_2-TPR). The reduction profiles of the catalysts were measured by hydrogen temperature programmed reduction (H_2-TPR) experiments employing a Micromeritics AutoChem II 2920 unit. The catalyst (50 mg) was placed on a quartz wool bed inside a quartz tube microreactor. The sample was pre-treated at 200°C in a flowing high-purity argon to eliminate water and impurities before it was cooled down to 50°C in flowing argon (50 mL.min^{-1}). Afterwards, the gas flow was switched to the reducing mixture (5 vol. % H_2 in Ar at a flow rate of 15 mL.min^{-1}) and the temperature was increased up to 900°C at a heating ramp of 10 °C.min^{-1}. The hydrogen consumption was monitored throughout the experiment with a thermal conductivity detector (TCD).

CO pulse chemisorption. The ruthenium dispersion was measured by CO pulse chemisorption using the same apparatus as described above for H_2-TPR experiments. The catalyst was reduced at 300 °C for 2 h in a reducing mixture (5 vol. % H_2 in Ar) with a flow rate of 50 mL.min^{-1}. After cooling down to 50°C, the gas flow was switched to helium (10 mL.min^{-1}) and these conditions were maintained for an additional 0.5 h. Then, CO was injected at regular intervals until the area of the peaks became constant. Assuming a CO:Ru stoichiometry of 1:1, ruthenium dispersion and metal area of Ru were calculated on the basis of the following equations :

$$\text{Ru dispersion, } D_{Ru}\ (\%) = \frac{n_{CO} \times SF \times MW \times 100}{C}$$

$$\text{Ru surface area, } A_{Ru}(m^2 g_{Ru}^{-1}) = \frac{n_{CO} \times N_a \times SF \times \sigma_m \times 10^{-18}}{C}$$

where n_{CO} is the chemisorption volume (mol g^{-1}), SF is the stoichiometry factor of CO to Ru = 1, C is the supported Ru metal weight (wt. %), MW is the molar weight of Ru = 101.1 g mol^{-1}, σ_m is the cross section area of Ru = 0.0614 nm^2 Ru atom^{-1} and N_a is the Avogadro's number.

X-ray photoelectron spectroscopy (XPS). The surface composition of the catalysts was analyzed by XPS using a Kratos Axis Ultra DLD apparatus equipped with a hemispherical analyzer and

a delay line detector. The spectra were recorded using an Al monochromated X-ray source (10 kV, 15 mA) with a pass energy of 40 eV (0.1 eV/step) for high resolution spectra, and a pass energy of 160 eV (1 eV/step) for survey spectrum in hybrid mode and slot lens mode, respectively. The C1s binding energy (285.0 eV) was used as an internal reference. Peak fitting and deconvolution of the experimental photopeaks was performed by CasaXPS software.

2.6. Hydrogenation catalytic tests

General procedure. The catalytic properties of the ruthenium-carbon catalysts were examined in the hydrogenation of various olefins using a 25 mL stainless-steel batch reactor (Parr instruments). Prior to the experiment, the catalyst was sieved and the fraction between 50 and 80 µm was used in order to minimize internal diffusion [51,52]. Then a given amount of catalyst (typically 25 mg) was pre-treated under H_2 flow (20 vol. % H_2 in N_2) for 2 h at 300 °C and cooled down to room in flowing nitrogen. Afterwards, the catalyst was contacted with 10 g of solvent (heptane) containing a precise amount of substrate. Then, dihydrogen was introduced in the autoclave until the pressure reached 40 bar. Next, the suspension was heated to 30 °C and stirred at 1250 rpm. The reaction was monitored by analysing aliquots of the reaction mixture using a gas chromatograph (Shimadzu GC-17A) equipped with a methyl silicone capillary column (30 m × 0.32 mm) and a flame ionization detector. Each catalytic run was performed in duplicate and the reported results are the average between the two runs with an experimental error of ± 2 %.

Reusability. For the recycling procedure, after the complete conversion of 1-decene, the catalyst was recovered by filtration and thoroughly washed with heptane and diethyl ether until complete elimination of the reaction product. After removal of the remaining diethyl ether under vacuum, the solid was reduced under H_2 at 300°C reloaded with the olefin and dihydrogen and reused in hydrogenation as described above.

3. Results and discussion

The main steps for the preparation of ruthenium-containing ordered mesoporous carbons synthesis by replication of SBA-15 silicas are graphically represented in Scheme 1.

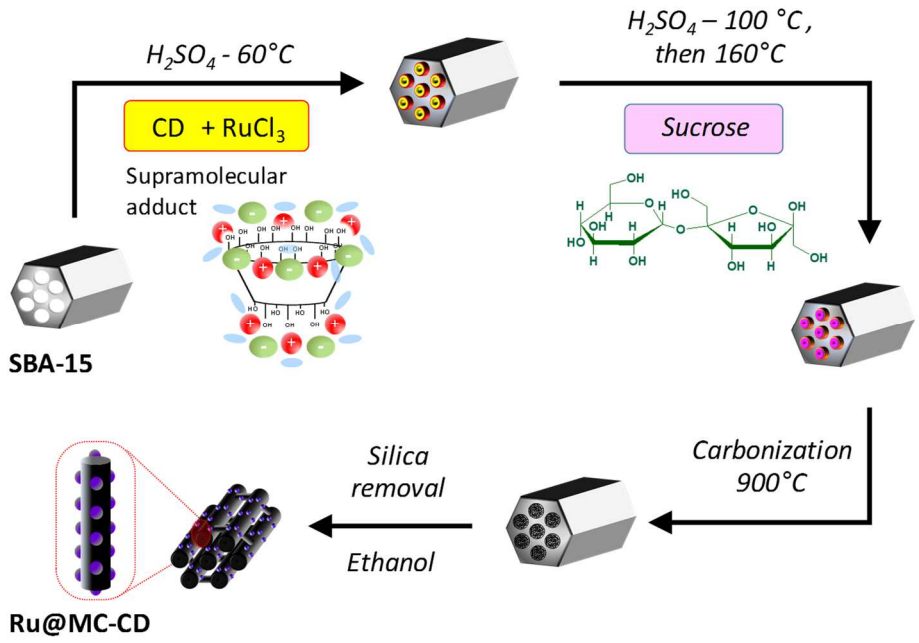

Scheme 1. Schematic illustration of the synthesis of Ru@MC-CD(x) by hard templating from supramolecular adducts formed between cyclodextrin and ruthenium trichloride.

The pore filling of the silica template is made in two times. The ruthenium salt precursor, i.e. $RuCl_3$, is added to cyclodextrin during the first impregnating step. The Ru:CD molar ratio in the solution has been set to values ranging from 1:10 to 5:10. Herein, the goal is to benefit from the multi-task ability of CDs (metal-complexing and thermo-reducing properties, and carbon source) within a single step. The physical confinement of the metal precursor is expected to limit the growth of the Ru particles within the layer formed by partially polymerized and carbonized cyclodextrin. The second impregnation step, which aims at filling up the pores of the template, is performed by using only an aqueous solution of sucrose (with no addition of ruthenium), followed by condensation/polymerization carried out under conventional thermal

conditions with regard to this specific organic source. Afterwards, the material is carbonized at high temperature and silica is finally removed in HF in order to obtain the ordered mesoporous ruthenium-carbon replica.

3.1. Textural and structural characterizations

The N_2 adsorption-desorption isotherms and pore size distributions (PSD) of the Ru-OMC samples prepared using CD (Ru:CD = 1:10) or using sucrose with exactly the same initial weight of ruthenium (4.55 mg for 600 mg of organic source) are plotted in Figure 1. The profiles of the SBA-15 template and MC-RAME control carbon replica (prepared without ruthenium) are given for comparison. We observe that all the isotherms obtained with this series of Ru-OMCs prepared with the lowest metal content (x = 1) can be classified as type IV with the presence of H2 type hysteresis loops at relative pressures of 0.4-0.85 typical of mesopores. The corresponding PSD confirm the presence of mesoporosity with average pore sizes ranging from 3.2 to 3.9 nm. As commonly observed with ordered mesoporous carbons synthesized with a hard-template, this range of size primarily originates from the void space formed after the removal of the ordered mesoporous SBA-15, which have a pore wall thickness estimated to approximately 4.2 nm (See the Experimental Section 2.2).

Table 1 lists the textural data from the N_2 adsorption analyses and shows that, for the carbon material and Ru-OMC samples (x = 1), high specific surface areas are maintained (1098-1234 $m^2.g^{-1}$, Table 1 entries 2-5), suggesting that they are only slightly affected by the nature of the carbon precursor. It can be noticed that, the addition of ruthenium to the saccharide impregnating solution results in an overall decrease in the mesopore volume. The drop seems more pronounced for the samples prepared with sucrose only, yielding values of about 32 % compared to that of the pure carbon. However, the contribution of micropores, which are inevitably formed by the gaseous species released during the pyrolysis step, is relatively low in

almost all carbon-based replicas (4-10%). This observation is in line with previous studies on biomass gasification over supported Ru/C catalysts, revealing that the presence of chlorides adsorbed on the ruthenium surface particles minimized gasification processes of the organic matter, and especially the methanation reaction by poisoning effect [53,54].

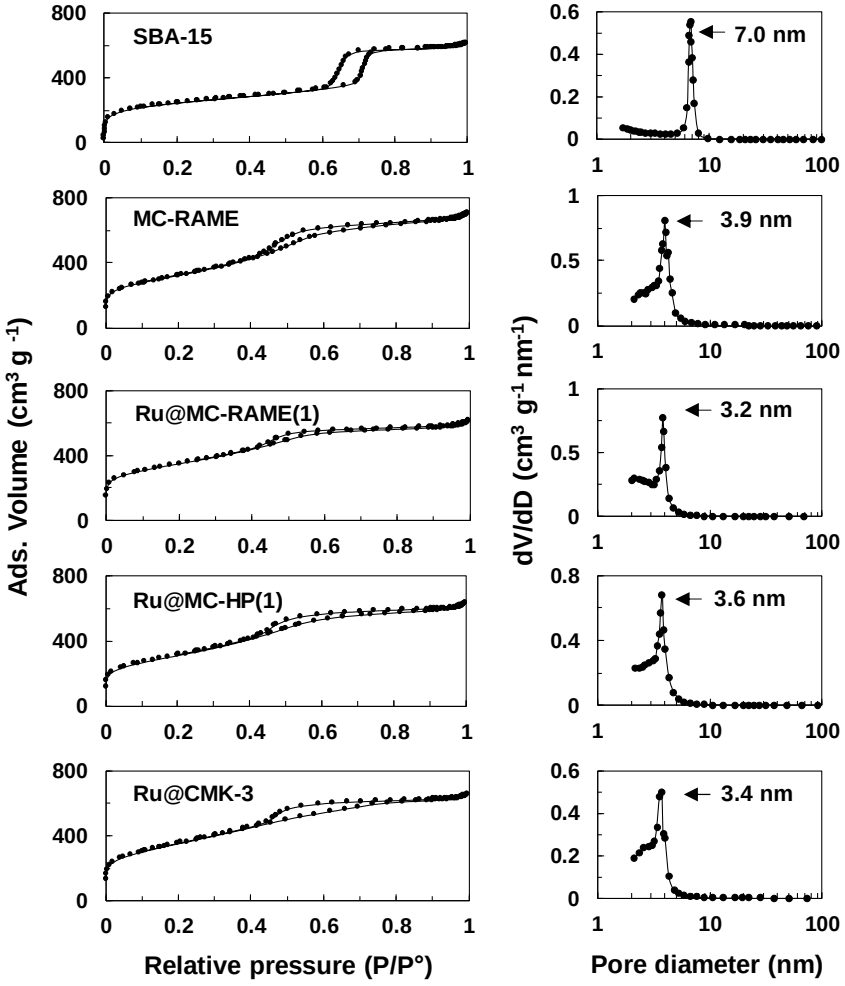

Figure 1. N_2 adsorption–desorption isotherms (left side) and pore size distributions (right side) of SBA-15, MC-RAME, Ru@MC-CD(1) and Ru@CMK-3 materials prepared with different sources of carbon at a fixed ruthenium to organic weight ratio of 4.55:600 mg.

Table 1. Textural properties of ruthenium-carbon catalysts prepared with different carbon sources and ruthenium loadings

Entry	Sample	Carbon precursor (1st. imp.)	Ru (mg) [a]	Ru/C [b]	d_{100} (nm) [c]	a_0 (nm) [d]	S_{BET} ($m^2\ g^{-1}$) [e]	V_P ($cm^3\ g^{-1}$) [f]	V_{micro} ($cm^3\ g^{-1}$) [g]	$\%_{micro}$ [h]	D_P (nm) [i]	Ru wt. (%) [j]
1	SBA-15	-	-	-	9.3	10.7	797	0.83	0.022	2.6	7.0	-
2	MC-RAME	RAME-β-CD	-	-	8.4	9.7	1130	1.22	0.053	4.2	3.9	-
3	Ru@MC-RAME(1)	RAME-β-CD	4.55	0.10	8.4	9.7	1234	0.95	0.044	4.4	3.2	1.7
4	Ru@MC-HP(1)	HP-β-CD	4.55	0.10	8.4	9.7	1098	0.90	0.045	4.8	3.6	1.2
5	Ru@CMK-3	Sucrose	4.55	0.025	8.3	9.6	1142	0.83	0.087	9.4	3.4	1.3
6	Ru@MC-HP(2)	HP-β-CD	9.22	0.20	8.6	9.9	1232	0.85	0.034	3.8	3.4	2.6
7	Ru@MC-HP(3)	HP-β-CD	13.8	0.3	8.7	10.0	1251	0.85	0.034	3.8	3.6	3.9
8	Ru@MC-HP(5)	HP-β-CD	23.0	0.50	8.8	10.2	1287	0.99	0.099	9.1	3.8	6.0

[a] Amount in weight of elementary ruthenium added to 600 mg of carbon precursor during the first infiltration step. [b] Nominal molar ratio of ruthenium to carbon precursor used for the first impregnation solution. [c] d-spacing calculated on the basis of the following formulas $n\lambda=2d_{100}\sin\theta$. [d] Unit cell constant calculated by the equation $a_0=2d_{100}/\sqrt{3}$. [e] Specific surface area calculated from the Brunauer-Emmet-Teller equation in the P/P^0 range of 0.025-0.20. [f] Total pore volume estimated at $P/P^0 = 0.95$. [g] Micropore volume determined by the t-plot method. [h] Percentage of micropore calculated as the ratio of micropore volume to total pore volume × 100. [i] Pore diameter determined by the Barrett-Joyner-Halenda method from the adsorption branch of the isotherm assuming cylindrical pores; [j] Ruthenium content in the final materials determined by ICP-OES.

Further experiments showed that the metal loading does not significantly affect the textural properties of the Ru-OMC materials. This study has been carried out by selecting HP–β-CD as cyclodextrin precursor respectively with metal-to-CD ratios ranging from 2:10 to 5:10. It should be noted above all that the loading percentages of noble metals in Ru-OMC materials have been determined by ICP-AES analyses, and the values evolve gradually from 2.6 to 6.0 wt.% with increasing the amount of Ru introduced in the synthesis. The metal loadings are fairly close to those estimated by assuming the complete transformation of the organic precursor into carbon, which indicates that the synthesis method provides a good control of the rates of metal incorporation in the finished materials without loss of metal.

In terms of textural properties, the shape of the adsorption isotherms of Ru@MC-HP(x) catalysts remains practically unchanged with the ratio, indicating an overall good preservation of the mesoporous properties of the carbon-based replicas (Figure S1, ESI). The specific surface area ranges from 1232 to 1287 $m^2.g^{-1}$ the pore volume from 0.85 to 0.99 $cm^3.g^{-1}$ and the pore size from 3.4 to 3.8 nm (Table 1 entries 6-8), these data being consistent with the general textural characteristics of the Ru-OMC solids with a low Ru content (x = 1) discussed above. However, it can be noticed that the proportion of micropores increases to some degree for Ru@MC-HP(5) (9.1 %) while it remains constant for Ru@MC-HP(2) and Ru@MC-HP(3) catalysts (3.8 %). The enhanced microporosity with the highest Ru loading suggests a slight deterioration of mesostructure ordering, maybe due to the presence of a high number of contact points between Ru and C atoms generating more gas released during the carbonization process.

The structural arrangement of the carbon nanostructures Ru-OMC materials was investigated by low-angle XRD analysis. Figure 2 plots the patterns for the Ru@MC-CD(1) and their respective controls. The low-angle XRD pattern of the mesoporous carbon material prepared

from RAME-β-CD shows a main (100) diffraction peak at 2θ ~1.05° and two weaker (110) and (200) features at higher 2θ values ~1.6° and 1.85° (indicated by the red arrows in the inset figure). These overall characteristics are indicative of a mesoporous structure having a 2-dimensional hexagonal symmetry similar to that of the ordered mesoporous SBA-15 silica (P6*mm*). Note that, compared to the silica template, the diffraction peaks of the mesoporous carbon replica are broader and slighted shifted to higher 2θ values, due to structural distortion and lattice shrinkage that occurs in the 2D-hexagonal-packing carbon nanorods after the silica removal.

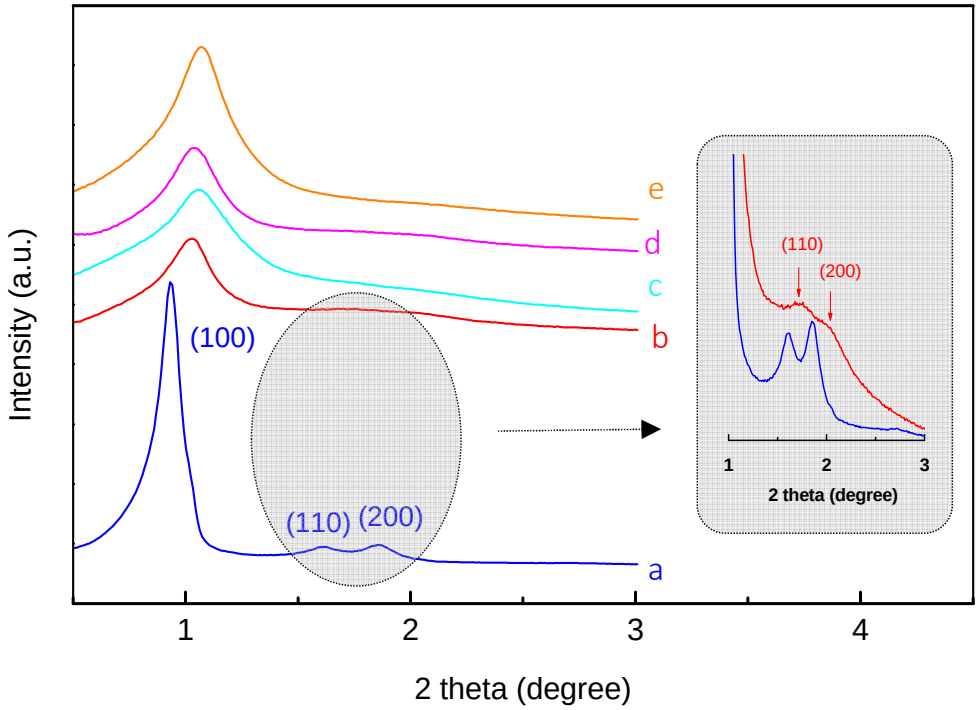

Figure 2. Low-angle XRD patterns of the following materials (a) SBA-15, (b) MC-RAME, (c) Ru@MC-RAME(1), (d) Ru@MC-HP(1) and (e) Ru@CMK-3.

With the incorporation of ruthenium chloride during the synthesis process, all the ruthenium-loaded carbon samples show similar diffraction patterns, with the presence of an intense (100) diffraction peak at 2θ values in the range of 1.05-1.07°. The unit cell parameters of the carbon-

based replicas deduced from the d_{100} spacing are given in Table 1. The resulting values are in a rather narrow range between 9.6 and 9.7 nm (Table 1 entries 2-5). However, the absence or quasi-absence of the higher order (110) and (200) peaks of hexagonal structure as well as the decrease in intensity of the (100) peak indicate that the presence of Ru NPs interferes with the long-range order of the carbon nanorods channels. This effect is particularly noticeable when the Ru-OMC materials are synthesized from RAME-β-CD or HP-β-CD compared to those from sucrose (compare patterns c and d with pattern e in Figure 2). Low-angle XRD measurements carried out on Ru@MC-HP(*x*) with increasing Ru loading corroborate this trend, exhibiting a decrease in intensity of the (100) peak, associated with the presence of more defects due to the interaction between the ruthenium nanoparticles and the carbon framework (Figure S2, ESI).

3.2. Transmission Electron Microscopy (TEM)

Figure 3 shows the representative TEM images of the Ru-OMC samples prepared from different carbon sources (with a low metal content ~ 1.2-1.7 % Ru). As an illustrative example, the TEM images of Ru@MC-RAME(1) show the cross section views of the carbon framework in the parallel and perpendicular direction to the channels (Figures 3a and 3b). Well-ordered hexagonal arrays of carbon nanorods separated by mesoporous channels are obtained, confirming that this sample prepared from RAME-β-CD and $RuCl_3$ has a 2D hexagonal structure (P6*mm*). From the bright-dark contrast of image (inset of Figure 3b), the size of the carbon nanorods is estimated to be in the range of ~6-7 nm, which is close to the pore diameter of the SBA-15 mesoporous hexagonal silica. At a higher magnification, it is possible to visualize the presence of small Ru NPs (black dots) nicely dispersed within the carbon framework of the catalyst (Figure 3c). As shown in the corresponding histogram, the average Ru size is 1.1 nm ± 0.3 nm and its size distribution is narrow with more than 80 % of nanoparticles ranging from 1 to 1.5 nm. However, similar particle size distributions are obtained independently of the nature of the carbohydrate source (i.e. RAME-β-CD, HP-β-CD or sucrose)

by using $RuCl_3$ as the metal salt (compare histograms of Figure 3c to 3e). Indeed, we observe that the Ru NPs are well distributed on the carbon surface, without showing any sign of aggregation. Thus, no particle larger than 2 nm has ever been seen on the images.

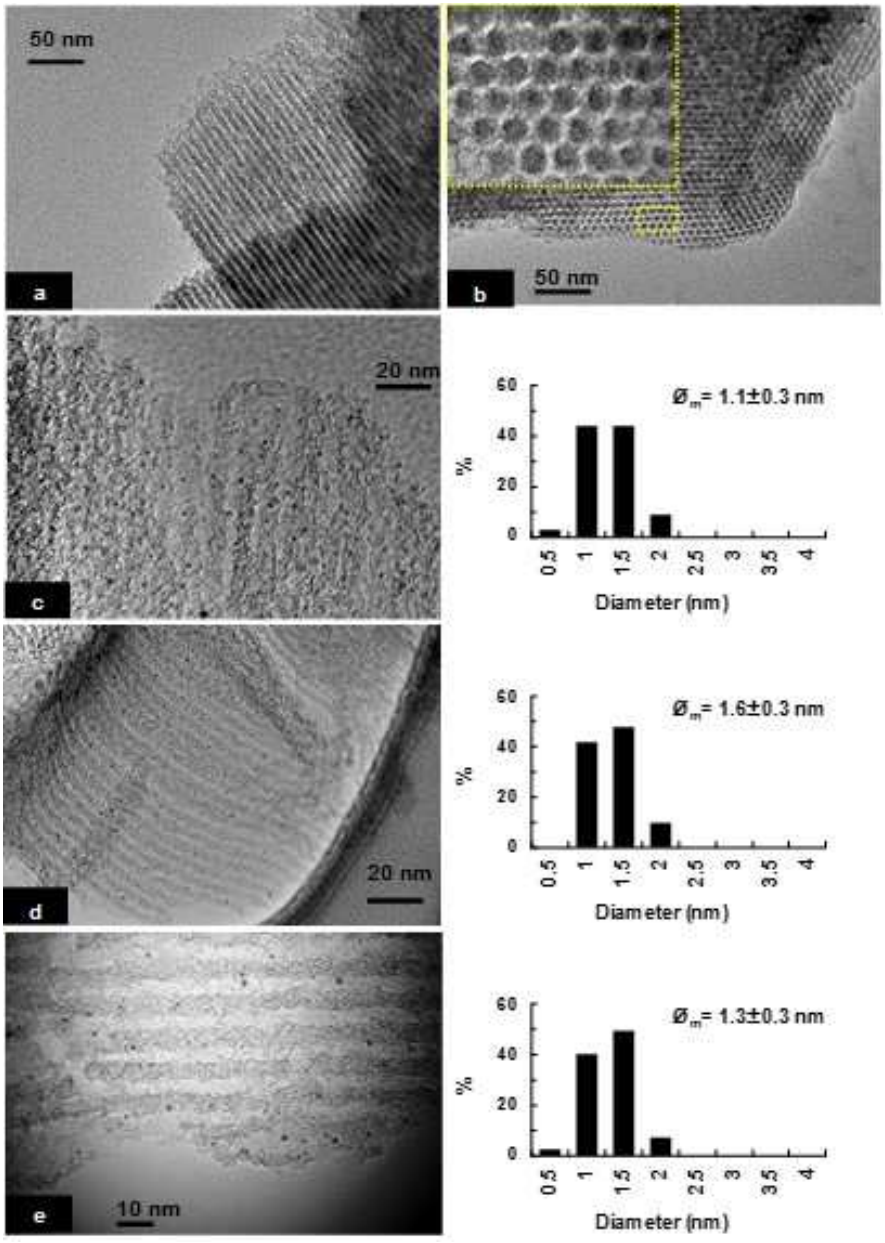

Figure 3. TEM images of Ru@MC-CD(1) and Ru@CMK3 composites at different magnifications and their corresponding particle size distributions (obtained from the measurement of ca. 200 particles): (a)&(b) Ru@MC-RAME(1), (c) Ru@MC-RAME(1), (d) Ru-A@MC-HP(1) and (e) Ru-@CMK-3.

The TEM study was further extended to Ru@MC-HP(x) catalysts with increasing Ru loadings (from 1.2 to 6.0 wt.%) (Figure S3, ESI). The images confirm that the introduction of greater amounts of ruthenium does not result in any appreciable change in the ordered structure of the carbon replicas after carbonization and silica removal. The carbon structures appear to be composed of arrays of long, straight or curved carbon nanorods aligned in 2D hexagonal arrays (images a, b and c, Figure S3, ESI). However, there is also evidence of coexistence of a more disordered structure over which Ru NPs are particularly prevalent. The majority of Ru nanoparticles are spherical in shape (images a', b' and c', Figure S3, ESI) and are relatively monodisperse with diameters ranging from 1 to 2.5 nm. Overall, the different TEM results support the fact that the oligosaccharide precursors, such as HP-β-CD, act as protecting agents to stabilize small ruthenium nanoparticles by preventing their aggregation throughout the whole synthetic process. The absence of large ruthenium aggregates is further confirmed by wide-angle XRD analysis, irrespective of the metal loading (Figure S4, ESI). Indeed, none of the diffraction peaks characteristic of Ru crystallites [2θ = 38.4° (100), 42.1° (002), 44.0° (101) and 58.3° (102) (JCPDS File No.06-0663)] and RuO_2 crystallites [2θ = 28.0° (110), 35.0° (011) and 54.2 (211) (JCPDS File No.40-1290)] is visible on the patterns. In addition, the low intensities of the C (002) reflexion may indicate an overall lack of graphitic ordering within the carbon frameworks.

3.3. CO pulse chemisorption

The Ru-OMC composites prepared from the different carbon precursors were analysed by CO pulse chemisorption in order to estimate the Ru metal dispersion and Ru surface area per gram of Ru metal (Table 2). All calculations were performed assuming an adsorption stoichiometry of one CO molecule per exposed ruthenium surface atom [55,56]. When the metal loading is in the low range (Ru < 2 wt. %), the results reveal that the Ru dispersion is greater for the catalysts prepared by reaction of $RuCl_3$ with RAME-β-CD or HP-β-CD (Table 2 entries 1 and 2). Indeed,

high levels of dispersion of 67 % and 72 % can be achieved for Ru@MC-RAME(1) and Ru@MC-HP(1), corresponding to large exposed surface areas (245 and 263 $m^2_{Ru}.g^{-1}_{Ru}$, respectively). The further increase in the Ru loading (from 2.6 to 6 wt. %) leads to a gradual decrease in the metal dispersion (from 72 to 47 %, Table 2 entries 4-6), but without being excessive as compared to that reported in the literature for typical Ru/AC catalysts prepared by impregnation of $RuCl_3$ solutions [57]. The significantly lower dispersion of Ru@CMK-3 made from sucrose (54%, Table 2 entry 3), which was difficult to predict only from the small particles observed in Figure 3-e, could be associated either with agglomeration effects of Ru particles on the carbon surface not visible in the TEM images or with substantial embedding of the metal nanoparticles in the carbon matrix.

Table 2. Surface chemistry of the ruthenium-carbon catalysts prepared with different carbon sources and ruthenium loadings

Entry	Sample	CO uptake ($\mu mol.g^{-1}$) [a]	Disp. (%) [b]	Metal surface area ($m^2.g_{Ru}^{-1}$) [c]	H_2 uptake ($\mu mol.g^{-1}$) [d]	H_2/CO ratio[e]
1	Ru@MC-RAME(1)	113	67	245	400 (167)	3.54
2	Ru@MC-HP(1)	85	72	263	391 (202)	4.60
3	Ru@CMK-3	69	54	196	265 (155)	3.84
4	Ru@MC-HP(2)	166	64	236	761 (nd)	4.58
5	Ru@MC-HP(3)	192	50	182	1025 (nd)	5.34
6	Ru@MC-HP(5)	280	47	172	1667 (nd)	5.95

[a] Estimated from the area under the CO pulse signals. [b] Calculated from the CO uptake using the equation: (n_{CO}*SF*MW *100)/C where n_{CO} is the amount of CO uptake ($mol.g^{-1}$), SF is the stoichiometric factor (Ru/CO =1), MW. is the molar weight of supported Ru (101.1 $g.mol^{-1}$) and C is the Ru loading (wt. %). [c] Calculated from the equation: (n_{CO}*N_A*SF*σ_m.*10^{-18})/C where N_A is the Avogadro number and σ_m is the Ru cross section area (0.0613 nm^2 $atom^{-1}$).[d] Estimated by integrating the H_2-TPR profile from 45 to 300°C. The numbers in brackets represents the H_2 uptake for the first reduction peak (when it is visible); nd, not detectable. [e] Defined as the ratio of the H_2 uptake measured by H_2-TPR per gram to the CO uptake per gram measured by CO pulse.

3.4. Thermogravimetry-Mass Spectrometry (TG-MS).

As there seems to be no evident relationship between the mean Ru particle size (determined by TEM) and the metal dispersion (determined by CO chemisorption), other parameters may be involved to explain the lack of correlation, such as the degree of carbonization of the precursors. The latter could be of importance for maintaining a good balance between incorporation and surface availability of the size-controlled Ru NPs. In this context, TG-MS analysis was employed to follow the changes occurring during the temperature-programmed carbonization process. Figure 4 reports the TG profiles and related derivative curves measured on four selected dried composites, i.e. SBA-15/Ru@sucrose, SBA-15/Ru@RAME(1), SBA-15/RAME and SBA-15/Ru@HP(1), all being recovered after the first infiltration step (see Scheme 1). In parallel, Figure S5 (see the Experimental Section) plots the main MS ion currents of the volatile substances emitted during the same heating program.

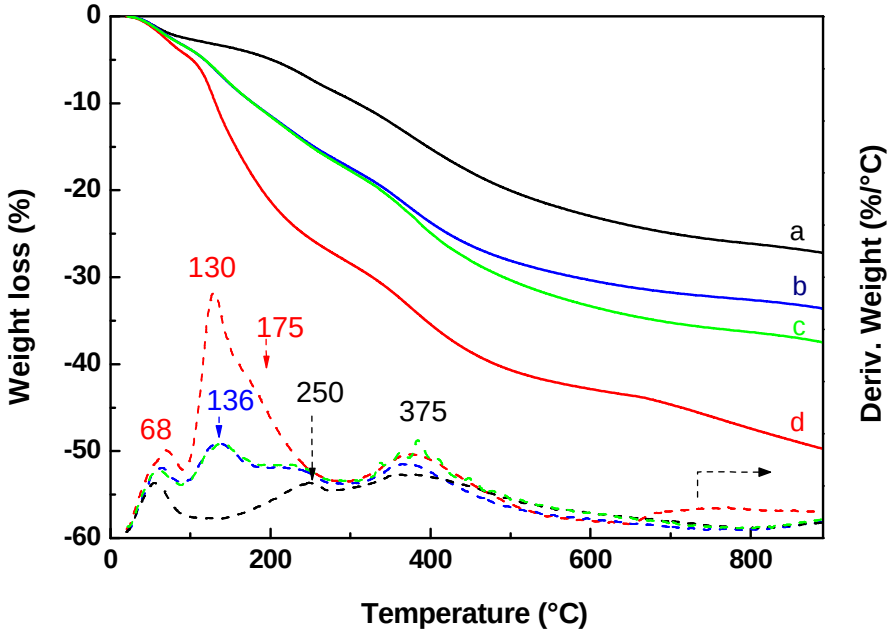

Figure 4. Thermogravimetric (TGA) and first derivative (DTG) profiles obtained under inert atmosphere (helium) of the following dried composites: (a) SBA15/Ru@sucrose, (b) SBA15/Ru@RAME(1), (c) SBA15/RAME and (d) SBA15/Ru@HP(1). The evolved gaseous compounds were monitored by on-line mass spectrometry (see Figure S5).

All the thermograms exhibit moderate weight losses (2-5 %) below 100°C, which are attributed to the departure of residual physically adsorbed water (m/z =18) from the precursors. These results are consistent with the fact that the major portion of this weakly bound water was previously eliminated during the sample preparation. Once the temperature exceeds 120°C, the process of pyrolysis begins and noticeable differences in the rate of decomposition can be observed depending on the carbon precursors. For sucrose (Figure 4, profile a), the weight loss curve is smooth, without showing any abrupt changes. The total weight loss reaches about 27% at 900°C. The corresponding MS results (Figure S5, A) show that H_2O is the dominant volatile species at T ~ 240°C, indicating that the chemical dehydration reactions are the main contributors to weight loss. This observation is in good agreement with the profile of the DTG curve in the low-temperature region of the TG-MS pattern (250°C).

At higher temperatures, the MS profiles of CO_2 (m/z = 44) and CO (m/z = 28) follow an overall similar trend, which suggest that they are simultaneously formed during pyrolysis, with two maxima positioned at 382°C and 465°C, respectively (Figure S5, B). The former can be preferentially generated by the cracking and reforming of functional carboxyl groups (COO) while the latter by the cracking of carbonyl (C=O) and ether groups (C-O-C) [58]. The signal m/z = 15 (580°C), which appears at higher temperatures than that of CO_2 and CO can probably be attributed to CH_3 coming from methane by degradation of primary unstable volatile species. In the high-temperature region above 650°C, the occurrence of extensive secondary reactions taking place in tar and char, such as steam reforming, is assumed to be responsible for the late production of H_2 (m/z = 2) and CO.

When substituting the sucrose for the RAME-β-CD as the carbon precursor, the onset of dehydration and maximum rate of water loss are abruptly shifted to lower temperatures (Figure

4, profiles b and c). The DTG peaks appear at 136°C, whether with or without $RuCl_3$, in good accordance with the water evolutions assigned to ion m/z = 18 from the TG-MS data (Figure S5, C and E). This feature upon the dehydration stage is even much more pronounced in the case of the HP-β-CD, showing a marked increase in the ion intensity of H_2O at 130°C (Figure S5, G). Note that the departure of water is also closely followed by a strong release of CO_2 and CO. Indeed, the CO_2 profiles measured from the composites exhibit two distinct signals (i.e., 150°C and 380°C for RAME-β-CD, and 165°C and 378°C for HP-β-CD). With regards to CO, except that there are some clear differences in the high-temperature region due to secondary pyrolytic reactions (T> 650°C), its releasing is similar to that of CO_2 with the presence of two main domains (150 and 410-420°C for RAME-β-CD, and 160°C and 400°C for HP-β-CD*).*

From these results, it appears that, compared to sucrose, these two modified CDs show similar decomposition properties, characterized by a faster conversion rate. However, among these two β-CD derivatives, HP-β-CD seems to be the most effective candidate for decomposition since the solid residue remaining after carbonization at 900°C was the lowest (50.2 wt.%). The differences in the chemical structure possibly accounts for the different behaviour observed. Sucrose is a disaccharide, composed of glucose and fructose (without branching) and crystalline in nature. Conversely, HP-β-CD and RAME-β-CD are chemically modified derivatives, where some hydroxyls are partially substituted by 2-hydroxypropoxy and methoxy groups, respectively (i.e., 4.2 $-OCH_2CH(OH)CH_3$ and 12.6 $-OCH_3$ per β-CD on the C2, C3 and C6 positions). They may appear as random and amorphous materials, with side groups that are easy to remove from the rim of β-CD by hydrolysis. This probably explains why more severe dehydration effects are observed at low temperature (T ~ 130°C), which in turn results in more rapid chemical bond cleavage and ring opening of the glucose units, and finally leads to lightly oxygenated carbon-based materials through the elimination of volatiles (i.e., H_2O, CO, CO_2 and

some other light gases, such as CH_4 and H_2). The greater amount of released gases for the HP-β-CD is likely related to the larger number of hydroxyl groups present in its structure, and in particular on its alkyl arms (4.2 2-OH *vs*. 0 for RAME-β-CD). As stated above, these hydroxyls can easily undergo dehydration to generate water (and/or hydronium due to acidic conditions) and accelerate the overall pyrolysis process. Taken together, these results indicate that the pyrolysis characteristics may have a functional role in the control of the carbon properties, but also in the dispersion of the metal nanoparticles. Indeed, as mentioned above, the best metal dispersion was measured for the HP-β-CD (72%) whose structure seems more appropriate for the fast pyrolysis. However, it is worth mentioning that surface exposure of Ru nanoparticles can be further enhanced by the removal of the silica template.

3.5. Temperature programmed reduction (H_2-TPR)

H_2-TPR was further employed to evaluate the reducibility of the catalysts. TPR profiles for Ru@CMK-3, Ru@MC-HP(1) RuMC-RAME(1) and MC-RAME are presented in Figure 5. For the ruthenium-free MC-RAME, no H_2 consumption peak appears for temperatures below 550°C (profile a). The high H_2 consumption, which is observed at higher temperatures (675°C) may be related to methanation or partial carbon gasification by H_2. It is worth noting that, for the Ru-OMC samples, the position of this band is significantly shifted to lower temperatures (590°C), and its intensity is also greatly enhanced (profiles b-d). These changes are indicative of stimulation of the carbon gasification process, probably occurring in the vicinity of metal particles. Note that this effect seems even more pronounced in the case of the sample prepared from HP-β-CD (profile d).

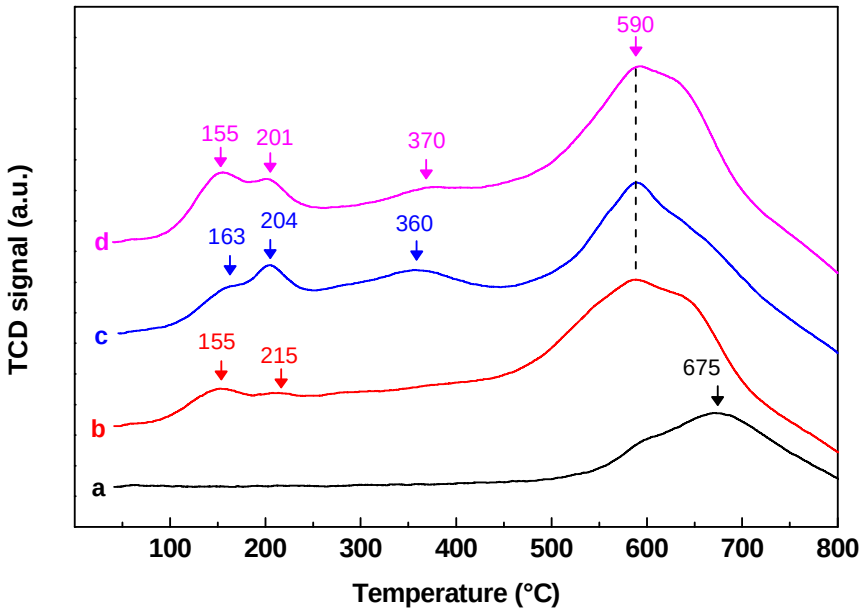

Figure 5. H_2-TPR profiles of Ru@CMK-3 (profile b), Ru@MC-RAME(1) (profile c) and Ru@MC-HP(1) (profile d) composites prepared without or with assistance of cyclodextrin. For comparison, the H_2-TPR profile of ruthenium-free carbon matrix, i.e. MC-RAME, is also included (profile a).

With the incorporation of Ru in the carbon matrix, the H_2-TPR profiles become also more complex in the low-temperature region (range 100-300°C), exhibiting two additional H_2 consumptions at about 155°C and 200°C. These signals are likely associated with the reduction of RuO_2 to Ru (0) in different environments, anticipating different types of metal carbon interactions. Even though Ru can be reduced in its metallic form upon thermal auto-reduction process, a portion of surface metallic Ru is sensitive to oxidation and can be oxidized when exposed to ambient air during the storage [59]. The precise attribution of the two reduction peaks is not straightforward, but similarly to what reported for metal-supported carbon materials, the first feature (~ 155°C) can be related to the reduction of well-dispersed (small) RuO_2 species bound to the external carbon surface, whereas the second one (~ 200°C) can be attributed to Ru species in intimate contact with the carbon network (partially or semi

embedded). In a quantitative viewpoint, we observe that the H_2 consumption corresponding to the first reduction band is significantly higher for the Ru-OMC sample prepared from HP-β-CD compared to that prepared from RAME-β-CD or from sucrose (202 *vs* 167 and 155 µmol g^{-1}, respectively), thus reflecting the presence of a greater density of surface Ru species. In the case of Ru@MC-RAME(1) and Ru@MC-HP(1), the TPR profiles exhibit also a shoulder band at approximately 360 and 370°C, respectively, which could be indicative of hydrogen spillover effect from Ru(0) to carbon. This is possibly linked to the existence of more Ru-carbon contacts, known to facilitate the transport of hydrogen atoms into the carbon sublayer [60]. Notably, this seems to be conditioned by the nature of the carbon precursor used during the preparation (i.e. see the intensity variation of the second band that almost vanishes for Ru@CMK-3). Unfortunately, attempts to detect difference in the surface properties of the Ru-OMC catalysts and identify a trend in terms of Ru-C contacts by X-ray photoelectron spectroscopy (XPS) were ambiguous, mainly because the C 1s peak covers the Ru $3d_{3/2}$ signal and partially overlaps the Ru $3d_{5/2}$ peak. The core-level peak of Ru 3p in carbon materials is generally chosen for XPS analysis, but it is less sensitive to the changes in the oxidation state than Ru 3d. (Figure S6, ESI).

3.6. Hydrogenation tests

Taken together, the characterization results presented above outlines that the nature of the carbon precursor plays a significant role in affecting the dispersion state and reduction behavior of ruthenium species anchored to ordered mesoporous carbons (even though the particle size distribution shows little variation, i.e. 0.5 – 2 nm). This can be clearly visualized for Ru@MC-HP(1). On the one hand, the CO pulse chemisorption measurements clearly point out a higher metal dispersion (72 %) and metal surface area (263 $m^2.g^{-1}$). On the other hand, the use of HP-β-CD in the first impregnation step enhances the reduction of surface RuO_2 species, as shown by H_2-TPR. Among the two cyclodextrins studied, HP-β-CD is the one with the largest amount

of hydroxyl groups (21 OH groups in total against 8.4 for RAME-β-CD), and their presence can be a favorable factor for both the adsorption on the SBA-15 surface and the formation of supramolecular adducts with Ru(III) ions. Interestingly, the affinity of Ru for HP-β-CD has been further supported by ESI-MS analysis in positive mode showing the possible existence of a supramolecular adduct occurring between ruthenium (III) chloride and HP-β-CD in the form of an ion $[HP\text{-}\beta\text{-}CD+Ru+Cl]^{2+}$ at m/z 838.7688 corresponding to the substitution degree of 7. (Figure S7, ESI). This process does not seem possible in the case of dimethyl-β-cyclodextrin, as already reported by Stark et al. [61]. This might favor a good distribution of ruthenium species on the silica surface, resulting after polymerization, carbonization and silica removal, in dispersed and partially encapsulated Ru nanoparticles. Additionally, as previously evidenced by TG-MS experiments, we suggest that the dehydration of the secondary alcohol present in the 2-hydroxypropoxy groups is another driving force for undergoing more rapid crosslinking reactions and pyrolysis process. This phenomenon increases the quantity of VOCs emitted, leading to higher surface area of ruthenium.

To assess the effect of cyclodextrins on the catalytic properties of such Ru-OMC catalysts, the performances were initially examined in the hydrogenation of 1-decene, chosen as model molecule of long-chain olefins. Prior to reaction, all catalysts were pre-reduced under a H_2 flow for 2 h. According to the TPR experiments, 300°C was the temperature selected for the reduction treatment. Catalytic tests were performed in an autoclave at a hydrogen pressure of 40 bar and a temperature of 30°C, using heptane as solvent (typical substrate:metal molar ratio of 1000:1). The reaction was monitored by gas chromatography (Procedure detailed in the experimental section). However in order to fully evaluate the hydrogenation properties of our Ru-OMC composites prepared by hard-template, additional tests were also conducted on two control monometallic Ru/AC catalysts, using the same substrate-to-metal ratio (1000:1). These

two catalysts, namely 4.2Ru/AC-L3S (4.2 wt.% Ru) and 3.7Ru/AC-L3S-NaClO (3.7 wt.% Ru), were synthesized by liquid-phase impregnation and cationic exchange according to previously reported methods [62]. The commercial activated carbon (L3S, CECA, 900 $m^2.g^{-1}$) is used either as received or after being chemically treated with sodium hypochlorite to introduce oxygen functionalities. TEM examination of 4.2Ru/AC-L3S and 3.7Ru/AC-L3S-NaClO catalysts displays similar particle size distributions, with the majority of Ru nanoparticles being below 2 nm, in addition of some agglomerates (Figure S8, ESI).

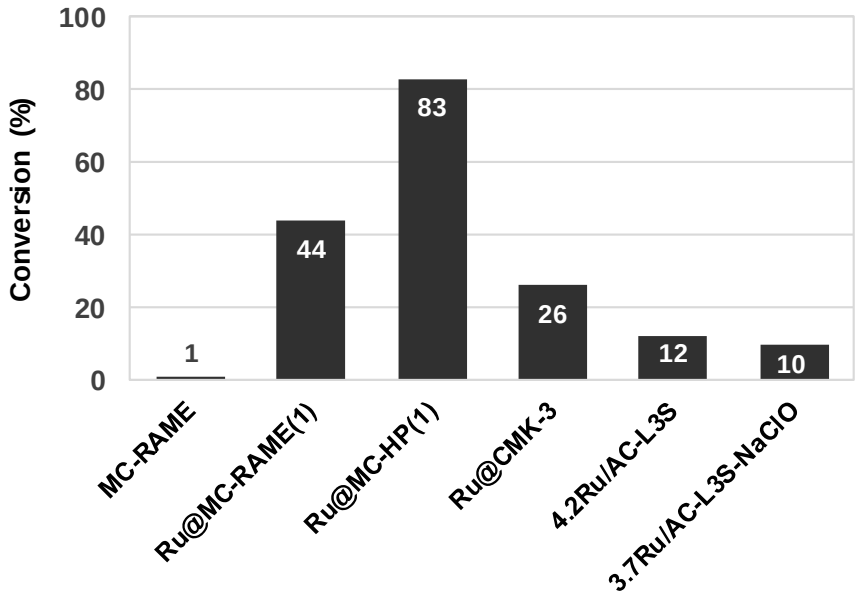

Figure 6. Performance of the different Ru-carbon catalysts prepared by hard-template or impregnation in the hydrogenation of 1-decene. Reaction conditions: Substrate:Ru, 1000:1; Pressure, 40 bar H_2; Temperature, 30°C; Time, 2 h; Stirring rate, 1250 rpm; Solvent, 10 g heptane. The number in the histogram indicates the conversion after 2 h reaction.

When comparing the conversion of 1-decene over the different catalysts after 2 h, it is readily apparent that the Ru@MC-HP(1) catalyst prepared by hard-template from the hydroxypropyl-β-CD show the highest activity, with ca. 85 % conversion after 2 h, decane being the only product observed (Figure 6). The conversion is about two times higher than Ru@MC-RAME(1)

(44 %) and three times higher than Ru@CMK-3 (26 %). The most significant effect in the model hydrogenation reaction achieved with the HP-β-CD-assisted catalyst (Ru:CD=1:10) can be explained on the basis of an excellent dispersion of Ru species, forming a homogeneous distribution of small Ru NPs in strong interaction with the carbon support. On the other hand, it is worth noting that the hard-template approach proves to be more efficient than the conventional liquid-phase impregnation. Thus, 4.2Ru/AC-L3S gives a much lower level of conversion of 1-decene (12 %) in the same experimental conditions. The use of the oxidized activated carbon to support the ruthenium active phase does not lead to any further improvement (10 % conversion). The latter two results suggest that factors other than Ru particle size and textural properties of the carbon structure play an important role in the hydrogenation activity. The interfacial characteristics of ruthenium-carbon could be another reason for the enhanced catalytic activity.

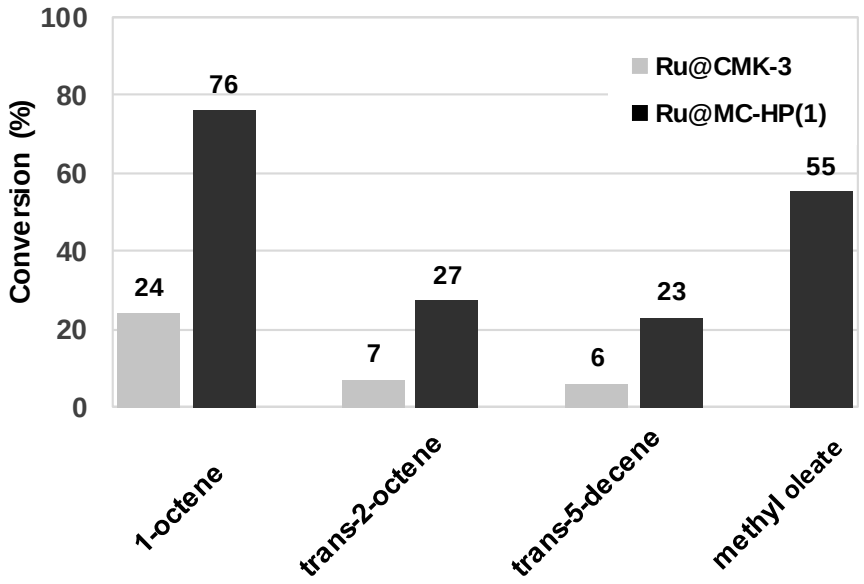

Figure 7. Performance of the Ru-carbon catalysts prepared by hard-template in the hydrogenation of various unsaturated substrates. Reaction conditions: Substrate:Ru, 1000:1; Pressure, 40 bar H_2; Temperature, 30°C; Time, 2 h; Stirring rate, 1250 rpm; Solvent, 10 g heptane. The number in the histograms indicates the conversion after 2 h reaction.

The novel Ru@MC-HP(1) catalyst was also found to be active for the hydrogenation of structurally diverse olefins, tested in the same experimental conditions as those previously described for 1-decene (T = 30 °C, PH_2 = 40 bar and t = 2 h) (Figure 7). It is clear from these results that Ru@MC-HP(1) is much more efficient than the control Ru@CMK-3, resulting in a threefold to fourfold increase depending on the substrate. Thus, hydrogenation of a shorter alkyl-chain olefin, namely 1-octene, yields 76 % conversion, without affecting the selectivity (100 % octane), which is comparable to that measured for 1-decene. Compared to 1-octene, the hydrogenation of the trans-2-octene internal C=C double bond proceeds more slowly, affording only 27% conversion within 2 h, presumably because of a lower adsorbability of the *trans* isomer on the metal active sites due to enhanced steric constraints. Similar results are also obtained with the trans-5-decene. In the hydrogenation of methyl oleate (C18:1, cis-9), selected as model compound of unsaturated fatty acid methyl esters, Ru@MC-HP(1) proves to be efficient for hydrogenating the olefinic C=C bond and producing the fully saturated methyl stearate (C18:0). The conversion reaches 55% within 2 h.

Given the promising catalytic properties of Ru@MC-HP(1), and keeping 1-decene as reactant, the reaction was further studied with various substrate-to-metal molar ratios, ranging from 300 to 10000. It is worth mentioning that the latter ratio, i.e. 10000:1, corresponds to a reaction performed under solvent-free condition, where no heptane was used. Conversions plotted as a function of time are shown in Figure 8. As expected, the results reveal appreciable differences in conversion when changing the substrate-to-metal molar ratio, the lower the ratio is, the higher the conversion is. The best results are obtained for the ratio of 300:1, with 96% of 1-decene converted within 1 h. Note that the initial slope was used to determine the initial activity, which is expressed as the number of 1-decene molecules converted per hour per mol of Ru. The results are gathered in Table 3.

Table 3. Performance of the different Ru@MC-HP(*x*) catalysts prepared from HP-β-CD (x varying from 1 to 5) for the hydrogenation of 1-decene.

Entry	Catalyst	Ru (mg)	1-decene:Ru	Solvent	t (h)	Conversion (%)	Initial activity (h^{-1}) [a]
1	Ru@MC-HP(1)	0.34	300:1	Heptane [b]	0.75	91	365
2	Ru@MC-HP(1)	0.34	1000:1	Heptane [b]	0.75	55	731
3	Ru@MC-HP(1)	0.34	10000:1	- [c]	1.5	18	1192
4	Ru@MC-HP(2)	0.71	10000:1	- [c]	1.5	18	1210
6	Ru@MC-HP(3)	0.96	10000:1	- [c]	1.5	22	1452
7	Ru@MC-HP(5)	1.44	10000:1	- [c]	1.5	32	2116

[a] initial activity: number of moles of 1-decene converted per mole of Ru per hour. The values are calculated from the Ru metal loadings determined by ICP measurements and from the metal dispersions (Disp) estimated by CO pulse chemisorption measurements. [b] Solvent mass is 10 g. [c] Experiment carried out under solvent-free conditions.

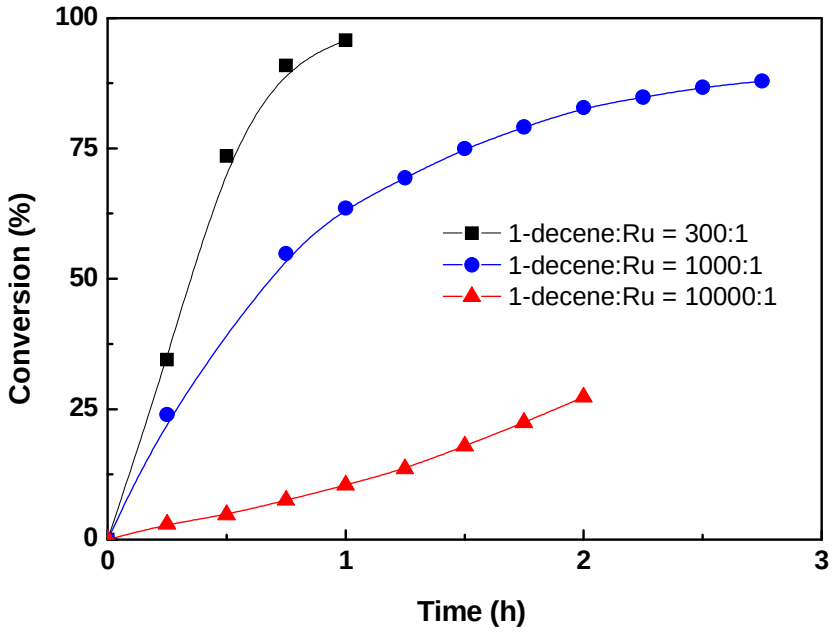

Figure 8. Conversion time plot for 1-decene hydrogenation with different substrate-to-molar ratios over Ru@MC-HP(1). Reaction conditions: Pressure, 40 bar H_2; Temperature, 30°C; Stirring rate, 1250 rpm; Solvent, heptane (except for the ratio of 10000:1which refers to solvent-free conditions).

Notably, the Ru@MC-HP(1) catalyst is able to preserve good performances even at high substrate concentration and without any additional solvent. Indeed, the activity normalized per mol of Ru present increases from 365 h^{-1} (Table 3 entry 1) to 1192 h^{-1} (Table 3 entry 3) with increasing the substrate/Ru molar ratio from 300 to 10000. Interestingly, this solvent-free procedure has been successfully applied to the other catalysts containing higher amounts of Ru. We observe that the conversion of 1-decene increases with the metal loadings (Table 3 entries 3-6). Thus, the highest activity is observed for Ru@MC-HP(5) with 32 % of 1-decene conversion after 1.5 h reaction (Table 3 entry 6).

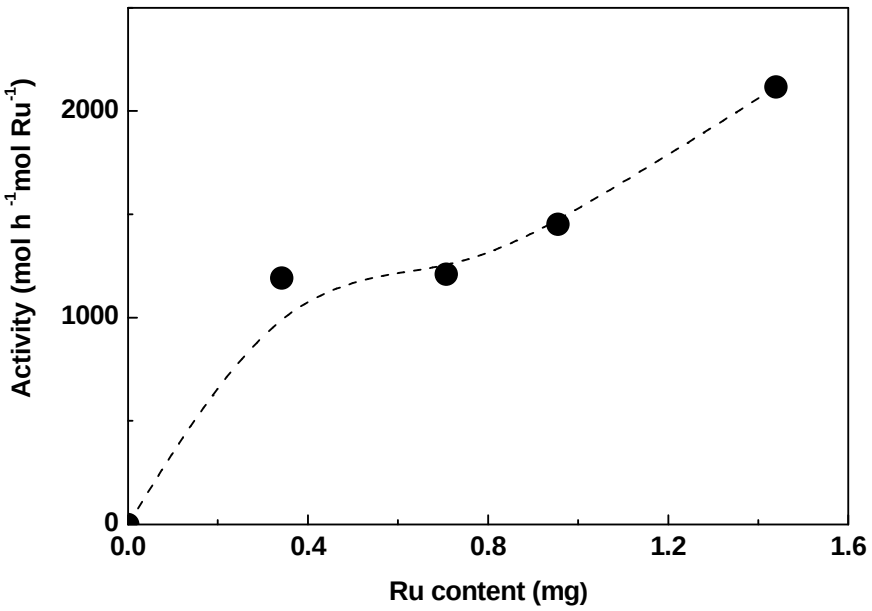

Figure 9. Effect of the Ru content on the initial activity in the hydrogenation of 1-decene measured for the different Ru@MC-HP(x) catalyst (*x* varying from 1 to 5) under solvent-free-conditions. Reaction conditions: Pressure, 40 bar H_2; Temperature, 30°C; Stirring rate, 1250 rpm.

In Figure 9, it is apparent that, at constant substrate-to-metal molar ratio, the hydrogenation initial activity tends to increase with the Ru loading. Such a trend suggests that there is a synergistic effect between the ruthenium NPs and carbon matrix on the rate enhancement of hydrogenation. Indeed, remembering that the average Ru particle size determined by TEM is relatively similar for each of the metal loadings, factors other than the metal dispersion must account for the enhancement of catalytic activity. With increasing the amount of Ru, it is expected an upward impact on the number of interfacial contacts between the Ru metal and the carbon phase (Ru-C linkages), which are known to exert a strong influence on hydrogenation reactions [21]. This effect can be promoted by our direct templated approach, involving the concomitant decomposition of $RuCl_3$ and HP-β-CD to form Ru@C nanostructures by thermal heating. In addition, the benefit of increasing the density of Ru NPs within the framework of

porous carbon can be also to promote hydrogen spillover effect. As mentioned earlier, hydrogen atoms can be readily generated on carbon-supported metal catalysts by dissociative adsorption of molecular hydrogen on the metal part and diffuse from the metal to the carbon support, forming a bound layer of mobile and reactive hydrogen [60]. Previous reports have also established the importance of building carbon bridges by carbonizing a precursor material for enhancing hydrogen spillover and storage capacity [63]. Higher Ru metal loadings may contribute to induce hydrogen-rich microenvironments by spillover from Ru to the carbon phase, and facilitate the transfer of hydrogen to the adsorbed 1-decene. Conversely, upon decreasing the Ru concentration within the carbon matrix, hydrogen uptake and hydrogen spillover are less prominent, thereby resulting in a lowering of the catalytic activity. These hypotheses are also consistent with our TPR results (Figure S9, ESI), which exhibit a gradual increase of the H_2 uptake in the low-temperature region (range 100 and 300°C) with the Ru loading. In order to gain more insight, the H_2-to-CO ratio has been determined by dividing the H_2 uptake (from H_2-TPR) by the CO uptake (from CO pulse chemisorption). Such a value can give an indication for each sample of the amount of stored H2 hydrogen by surface Ru species. Thus, our data indicate that all H_2/CO ratios are higher than 1 (as expected for a surface enriched by hydrogen spillover). In addition, when comparing the H_2/CO ratio, a higher value is observed for x = 5 as compared to x =1 (5.95 vs 4.60 respectively), suggesting a more favorable H_2 spillover from the metal to carbon.

3.8. Recycling experiments

To assess the potential of HP-β-CD for the development of stable ruthenium-carbon composite catalysts by hard-template, a recycling study was conducted on Ru@MC-HP(3) in the hydrogenation of 1-decene at 30°C and 40 bar H_2. After a first run with the reduced catalyst and complete conversion of 1-decene, the catalyst was subjected to washing with diethyl ether until complete elimination of the reaction product. After removal of the remaining diethyl ether

under vacuum, the solid was then reduced under H_2 at 300°C, reloaded with 1-decene and dihydrogen, and reused in hydrogenation in the same manner as in Run 1.

As shown in Figure 10, Ru@MC-HP(3) can be successfully recycled at least 4 times without losing its activity. In addition, the stability of this material was also validated by additional ICP-OES measurements. Thus, we observe that the concentration level of ruthenium in the organic phase after each run is in all case inferior to 0.5 ppm (corresponding to the limit value of quantification). This quantification clearly shows that no leaching of ruthenium occurs in the organic phase, proving the stability and robustness of Ru NPs incorporated in the carbon matrix during the reaction.

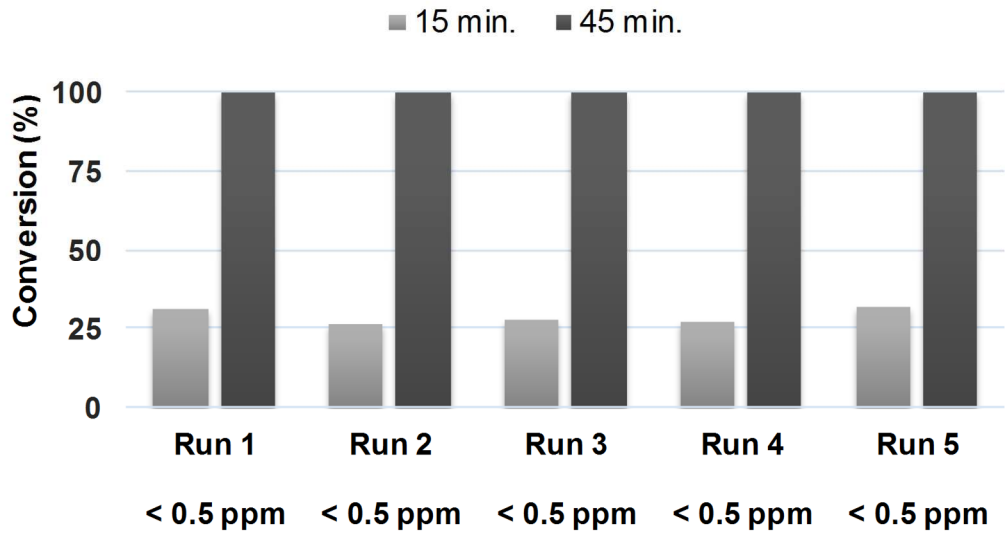

Figure 10. Reusability of Ru-A@MC-HP(3) catalyst in the hydrogenation of 1-decene after 15 and 45 minutes of reaction. Reaction conditions: Substrate:Ru, 300:1; Pressure, 40 bar H_2; Temperature, 30°C; Stirring rate, 1250 rpm; Solvent, 10 g heptane. Values at the bottom correspond to experimental Ru content determined after each test by ICP-OES measurements.

Moreover, the stability of the Ru@MC-HP(3) system has also been checked by TEM measurements. The images taken after the fifth run clearly show that the particle sizes and distribution are kept constant (Figure S10, ESI). Notably, the Ru(0) NPs displays a Gaussian-

like distribution and a mean diameter of 1.7 ± 0.4 nm with 90% between 1.0 and 2.0 nm, correlating well with the data obtained before catalysis (1.8 ± 0.4 nm, Figure S3, ESI). This last result further supports the observation made previously about the resistance of Ru NPs against aggregation and leaching under the catalytic conditions.

4. Conclusions

The fabrication of the sintering-stable ruthenium containing mesoporous carbonaceous catalysts was studied on the basis of the cyclodextrin-assisted hard-template approach. The specificity of the method relied on the direct infiltration of a mixture of β-cyclodextrin (methylated or hydroxypropylated) and $RuCl_3$ in controlled amounts into the pores of SBA-15. Upon carbonization, the ruthenium precursor became *in situ* reduced to form monodispersed Ru nanoparticles of ca. 1.0-2.0 nm, accompanied with the formation of a rigid mesoporous carbonaceous framework. After the removal of the silica template, the Ru@MC-CD catalysts present ordered mesostructures, high surface areas (~1100-1250 $m^2.g^{-1}$), large pore volume (~0.9 $cm^3.g^{-1}$), and uniform mesopore distribution (centered at ~3.5 nm), indicating little impact of the β-CD type on the textural properties. Conversely, our data revealed that the addition of $RuCl_3$ to cyclodextrin in the infiltration solution provided significant influence on the surface metal dispersion and hydrogen uptake behavior. On the basis of CO-pulse chemisorption and TPR measurements, the most noticeable effects were observed with the HP-β-CD, explained by its large presence of hydroxyls on the two edges of the molecule that could cooperate in the first steps of the synthesis with the ruthenium cations and silanols of the silica template. As a result, the Ru nanoparticles thus prepared exhibited remarkably high activity in the hydrogenation of 1-decene, and other olefin derivatives. This enhanced activity was attributed to a good balance between metal dispersion and hydrogen-spillover effect boosted by

intimate surface contact between the ruthenium and carbon phases. The catalysts are stable and reusable with no activity loss due to metal leaching.

Acknowledgements

This work was supported by the French Agency of Research (ANR) through the CYCLOMAT program (ANR 11-NANO-005). The authors also acknowledge the Chevreul Institute (FR 2638), Ministère de l'Enseignement Supérieur et de la Recherche, Region Hauts de France and FEDER program for supporting and partially funding this work. The TEM facility in Lille (France) is supported by the Conseil Regional des Hauts de France, and the European Regional Development Fund (ERDF). The authors warmly thank Dr. Nicolas Kania (UCCS, Univ. Artois) for his assistance for the H_2-TPR and CO-chemisorption analyses as well as Laurence Burylo, Olivier Gardoll and Martine Trentesaux (UCCS, Univ. Lille) for the XRD, TGA-MS and XPS experiments, respectively. The authors would like to express their gratitude to Dr. Cédric Przybylski from IPCM-CNRS (Sorbonne Universités, UPMC) for conducting the ESI-MS analyses.

References

[1] L. Chen, Y. Zhu, H. Zheng, C. Zhang, B. Zhang, Y. Li, J. Mol. Catal. A: Chem. 351 (2011) 217-227.

[2] H. Can, Ö Metin, Appl. Catal., B: Env. 125 (2012) 304-310.

[3] E. Gallegos-Suarez, M. Pérez-Cadenas, A. Guerrero-Ruiz, I. Rodriguez-Ramosa, A. Arcoya, Appl. Surf. Sci. 287 (2013) 108-116.

[4] E. Gallegos-Suarez, A. Guerrero-Ruiz I. Rodriguez-Ramos, A. Arcoya, Chem. Eng. J. 262 (2015) 326-333.

[5] P. Korovchenko, C. Donzé, P. Gallezot, M. Besson, Catal. Today 121 (2007) 13-21.

[6] A. Denicourt-Nowicki, A. Roucoux, F. Wyrwalski, N. Kania, E. Monflier, A. Ponchel, Chem. Eur. J. 14 (2008) 8090-8093.

[7] S. Iqbal, S A. Kondrat, D. R. Jones, D. C. Schoenmakers,J. K. Edwards, L. Lu, B. R. Yeo, P. P. Wells, E. K. Gibson, D. J. Morgan, C. J. Kiely, G. J. Hutchings, ACS Catal. 5 (2015) 5047−5059

[8] C. D. Taboada, J. Batista, A. Pintar, J. Levec, Appl. Catal. B: Env. 89 (2009) 375-382.

[9] S. Gil, L.Muñoz, L. S. Silva, A. Romero, J. L. Valverde, Chem. Eng. J. 172 (2011) 418-429.

[10] W. Han, L. Li, H. Yan, H. Tang, Z. Li, Y. Li, H. Liu, ACS Sustainable Chem. Eng. 5 (2017) 7195-7202.

[11] R. J. White, R. Luque, V. L. Budarin, J. H. Clark, D. J. Macquarrie, Chem. Soc. Rev. 38 (2009) 481-494.

[12] J. Schuster, G. He, B. Mandlmeier, T. Yim, K. T. Lee, T. Bein, L. F. Nazar, Angew. Chem. Int. Ed. 51 (2012) 3591-3595.

[13] N. Gokulakrishnan, N. Kania, B. Léger, C. Lancelot, D. Grosso, E. Monflier, A. Ponchel, Carbon 49 (2011) 1290-1298.

[14] J. Zheng, K. Wang, Y. Liang, F. Zhu, D. Wu, G. Ouyang, Chem. Commun. 52 (2016) 6829-6832.

[15] R. Ryoo, S. H. Joo, S. Jun, J. Phys. Chem. B 103 (1999) 7743-7746.

[16] J. Lee, S. Yoon, T. Hyeon, S. M. Oh and K. B. Kim, Chem. Commun. (1999) 2177-2178.

[17] C. Liang, Z. Li, S. Dai, Angew. Chem. Int. Ed. 47 (2008) 3696-3717.

[18] S. M. Holmes, P. Foran, E. P. L. Roberts, J. M. Newton, Chem. Commun. (2005) 1912-1913.

[19] F. Kerdi, V. Caps, A. Tuel, Microporous Mesoporous Mater. 140 (2011) 89-96.

[20] A.-H. Lu, W.-C. Li, Z. Hou, F. Schüth, Chem. Commun. (2007) 1038-1040.

[21] F. Su, L. Lv,, F. Yin Lee, T. Liu, A. I. Cooper, X. S. Zhao, J. Am. Chem. Soc. 129 (2007) 14213-14223.

[22] F. Su, F. Yin Lee, L. Lv,, J. Liu, X. N. Tian A, X. S. Zhao, Adv. Funct. Mater. 17 (2007) 1926-1931.

[23] Y. Li, G. Lan, H. Wang, H.Tang, X. Yan, H. Liu, Catal. Commun. 20 (2012) 29-35.

[24] G. Lan, H. Tang, Y. Zhou, W. Han, H. Liu, X. Li, Y. Li, ChemCatChem 6 (2014) 353-360.

[25] Z Jiang, G. Lan, X. Liu, H. Tang, Y. Li, Catal. Sci. Technol. 6 (2016) 7259-7266.

[26] K. Xiong, J. Li, K. Liew, X. Zhan, Appl. Catal. A: Gen. 389 (2010) 173-178.

[27] K. Xiong, Y. Zhang, J. Li, K. Liew, J. Energy Chem. 22 (2013) 560-566.

[28] G. Wenz, B. Keller, Angew. Chem. Int. Ed. 31 (1992) 197-199.

[29] J. Szejtli, J. Pure Appl. Chem. 76 (2004) 1825-1845.

[30] J R. Breslow, S. D. Dong, Chem. Rev.98 (1998) 1997-2011.

[31] A. Denicourt-Nowicki, A. Ponchel, E. Monflier, A. Roucoux, Dalton Trans. (2007) 5714-5719.

[32] S. Noël, B. Léger, A. Ponchel, K. Philippot, A. Denicourt-Nowicki, A. Roucoux, E. Monflier, Catal. Today 235 (2014) 20-32.

[33] R. Herbois, S. Noël, B. Léger,S. Tilloy, S. Menuel, A. Addad, B. Martel, A. Ponchel, E. Monflier, Green Chem. 17 (2015) 2444-2454.

[34] E. Norkus, J. Incl. Phenom. Macrocycl. Chem. 65 (2009) 237-248.

[35] L. X. Song, M. Wang, Z. Dang, F. Y. Du, J. Phys. Chem. B 114 (2010) 3404-3410.

[36] D. Prochowicz, A. Kornowicz, I. Justyniak, J. Lewinski, Coord. Chem. Rev. 306 (2016) 331-345.

[37] A. Jean-Marie, A. Griboval-Constant, A.Y. Khodakov, E. Monflier, F. Diehl, Chem. Commun. 47 (2011) 10767-10769.

[38] L. Bai, F. Wyrwalski, J-F. Lamonier, A. Khodakov, E. Monflier, A. Ponchel, Appl. Catal. B: Env. 138-139 (2013) 381-390.

[39] L. Bai, F. Wyrwalski, M. Safariamin, R. Bleta, J.F. Lamonier, C. Przybylski, E. Monflier, A. Ponchel, J. Catal. 341 (2016) 191-204.

[40] A. Tomer, F. Wyrwalski, C. Przybylski, J.-F. Paul, E. Monflier, M. Pera-Titus, A. Ponchel, J. Catal. 356 (2017) 111-124.

[41] B. H. Han, W. Zhou, A. Sayari, J. Am. Chem. Soc. 125 (2003) 3444-3445

[42] W. Shen, X. Yang, Q. Guo, Y. Liu, Y. Song, Z. Han, Q. Sun, J. Cheng, Mater. Lett. 60 (2006) 3517-3521.

[43] H. C. Wang, B. L. Li, J. T. Li, P. Lin, X. B. Bian, J. Li, B. Zhang, Z. X. Wan, Appl. Surf. Sci. 257 (2011) 4325-4330.

[44] N. Gokulakrishnan, G. Peru, S. Rio, J.-F. Blach, B. Léger, D. Grosso, E. Monflier, A. Ponchel, J. Mater. Chem. A 5 (2014) 6641-6648.

[45] V.N. Belyakov, L.A. Belyakova, A.M. Varvarin, O.V. Khora, S.L. Vasilyuk, K.A. Kazdobin, T.V. Maltseva, A.G. Kotvitskyy, A.F. Danil de Namor, J. Colloid Interface Sci. 285 (2005) 18-26.

[46] A. Tomer, B.T. Kusema, J.-F. Paul, C. Przybylski,, E. Monflier, M. Pera-Titus, A. Ponchel, J. Catal. 368 (2018) 172-189.

[47] B. L. Newalkar, S. Komarneni, H. Katsuki, Chem. Commun. 23 (2000) 2389-2390.

[48] M. Kruk, M. Jaroniec, Y. Sakamoto, O. Terasaki, R. Ryoo, C. H. Ko, J. Phys. Chem. B. 104 (2000) 292-301.

[49] S. Jun, S. H.Joo, R. Ryoo, M. Kruk, M. Jaroniec, Z. Liu, T. Ohsuna, O. Terasaki, J. Am. Chem. Soc. 122 (2000) 10712-10713.

[50] P. Korovchenko, C. Donzé, P. Gallezot, M. Besson, Catal. Today 121 (2007) 13-21.

[51] E. Santacesaria, Catal. Today 34 (1997) 411-420.

[52] A. Aho, S. Roggan, K. Eränen, T. Salmi, D. Y. Murzin, Catal. Sci. Technol. 5 (2015) 953-959.

[53] A. Yamaguchi, N. Hiyoshi, O. Sato, M. Osada, M. Shirai, Catal. Lett. 122 (2008) 188-195.

[54] A. Yamaguchi, N. Hiyoshi, O. Sato, M. Osada, M. Shirai, Energy Fuels 22 (2008) 1485-1492.

[55] L. Oliviero, J. Barbier Jr., D. Duprez, A. Guerrero-Ruiz, B. Bachiller-Baeza, I. Rodriguez-Ramos, Appl. Catal. B:Env. 25 (2000) 267-275.

[56] P. Seetharamulu, V. Siva Kumar, A.H. Padmasri, B. David Raju, K.S. Rama Rao, J. Mol. Catal. A: Chem. 263 (2007) 253-258.

[57] S. Galvagno, G. Capannelli, G. Neri, A. Donato, R. Pietropaolo, J. Mol. Catal. 64 (1991) 237-246.

[58] H. Yang, R. Yan, H. Chen, D.H. Ho Lee, C. Zheng, Fuel 86 (2007) 1781-1788.

[59] S-Y. Huang, S-M. Chang, C-t. Yeh, J. Phys. Chem. B 110 (2006) 234-239.

[60] P. C. H. Mitchell, A. J. Ramirez-Cuesta, S. F. Parker, J. Tomkinson, D Thompsett, J. Phys. Chem. B 107 (2003) 6838-6845.

[61] C. B. W. Stark, N. P. Lopes, T. Fonseca, P. J. Gates, Chem. Commun. (2003) 2732-2733.

[62] F. Kerdi, H. Ait Rass, C. Pinel, M. Besson, G. Peru, B. Léger, S. Rio, E. Monflier, A. Ponchel, Appl. Catal. A: Gen. 506 (2015) 206-219.